Liver Cancer

Research Article

Liver Cancer
DOI: 10.1159/000530645

Received: October 25, 2022
Accepted: April 3, 2023
Published online: April 14, 2023

Real-Time Fluorescence Imaging to Identify Cholangiocarcinoma in the Extrahepatic Biliary Tree Using an Enzyme-Activatable Probe

Ryugen Takahashi[a] Takeaki Ishizawa[a, b] Yoshinori Inagaki[a] Mariko Tanaka[c] Akira Ogasawara[d] Yugo Kuriki[d] Kyohhei Fujita[e] Mako Kamiya[e, f] Tetsuo Ushiku[c] Yasuteru Urano[d, e] Kiyoshi Hasegawa[a]

[a]Hepato-Biliary-Pancreatic Surgery Division, Department of Surgery, Graduate School of Medicine, The University of Tokyo, Bunkyo-ku Tokyo, Japan; [b]Department of Hepatobiliary-Pancreatic Surgery, Graduate School of Medicine, Osaka Metropolitan University, Osaka, Japan; [c]Department of Pathology, Graduate School of Medicine, The University of Tokyo, Tokyo, Japan; [d]Laboratory of Chemistry and Biology, Graduate School of Pharmaceutical Sciences, The University of Tokyo, Tokyo, Japan; [e]Laboratory of Chemical Biology and Molecular Imaging, Graduate School of Medicine, The University of Tokyo, Tokyo, Japan; [f]Department of Life Science and Technology, Tokyo Institute of Technology, Tokyo, Japan

Keywords
Cholangiocarcinoma in the extrahepatic biliary tree · Fluorescence imaging · Enzyme-activatable probe · Puromycin-sensitive aminopeptidase

Abstract

Introduction: Complete resection is the only possible treatment for cholangiocarcinoma in the extrahepatic biliary tree (eCCA), although current imaging modalities are limited in their ability to accurately diagnose longitudinal spread. We aimed to develop fluorescence imaging techniques for real-time identification of eCCA using an enzyme-activatable probe, which emits fluorescence immediately after activation by a cancer-specific enzyme. ***Methods:*** Using lysates and small tissue fragments collected from surgically resected specimens, we selected the most specific probe for eCCA from among 800 enzyme-activatable probes. The selected probe was directly sprayed onto resected specimens and fluorescence images were acquired; these images were evaluated for diagnostic accuracy. We also comprehensively searched for enzymes that could activate the probe, then compared their expression levels in cancer and non-cancer tissues. ***Results:*** Analyses of 19 samples (four cancer lysates, seven non-cancer lysates, and eight bile samples) and 54 tissue fragments (13 cancer tissues and 41 non-cancer tissues) revealed that PM-2MeSiR was the most specific fluorophore for eCCA. Fluorescence images of 7 patients were obtained; these images enabled rapid identification of cancerous regions, which closely matched histopathology findings in 4 patients. Puromycin-sensitive aminopeptidase was identified as the enzyme that might activate the probe, and its expression was upregulated in eCCA. ***Conclusion:*** Fluorescence imaging with PM-2MeSiR, which may be activated by puromycin-sensitive aminopeptidase, yielded generally high accuracy. This technique may be useful for real-time identification of the spread of eCCA during surgery and endoscopic examinations.

karger@karger.com
www.karger.com/lic

Correspondence to:
Kiyoshi Hasegawa, hasegawa-2su@h.u-tokyo.ac.jp
Yasuteru Urano, uranokun@m.u-tokyo.ac.jp

Introduction

Radical resection remains the primary curative treatment for cholangiocarcinoma in the extrahepatic biliary tree (eCCA), although its surgical procedures (e.g., extended hemi-hepatectomy and/or pancreaticoduodenectomy) are associated with high risks of serious complications [1–3]. To achieve curative effects while ensuring surgical safety, it is essential to determine bile duct resection locations based on the findings of pre-/intraoperative imaging studies and pathological examinations [4, 5]. Despite advances in imaging and endoscopic techniques, however, diagnostic accuracy remains unsatisfactory [6–8] because cancer tissues can spread along superficial layers of bile ducts [9]; moreover, it is often difficult to distinguish cancer cells from inflammatory changes caused by cholangitis and/or the placement of biliary drainage tubes.

We developed a unique fluorescence imaging technique that enables real-time identification of cancer tissue using enzyme-activatable fluorescence probes [10]. In this technique, a non-fluorescence probe (i.e., a fluorophore and a substrate such as a dipeptide or glucose) is hydrolyzed by a cancer-specific overexpressed enzyme and internalized by cancer cells, which enables real-time fluorescence-mediated detection of cancer tissue. Thus far, various enzyme-activatable fluorescent probes have been developed [11–14] and applied to the identification of breast cancer [13, 15, 16], esophageal cancer [12, 17], lung cancer [14, 18], head and neck cancer [19], and glioblastoma [20].

In the field of hepatobiliary and pancreatic surgery, we have demonstrated that fluorescence imaging using gGlu-hydroxymethyl rhodamine-green (HMRG) and GP-HMRG can visualize primary/metastatic liver cancers [21] and pancreatic cancer [22], respectively. These enzyme-activatable probes, designed for topical administration on tissue surfaces, have the potential to delineate the longitudinal spread of cholangiocarcinoma.

In this study, we explored our library of 800 probes to identify a candidate enzyme-activatable fluorescence probe selective for eCCA. We also identified an enzyme with cholangiocarcinoma-specific overexpression, which might activate the probe; this enzyme is a potential target for the development of additional novel imaging and therapeutic reagents.

Materials and Methods

Study Design

First, the probe most specific for cholangiocarcinoma was selected by analysis of surgically resected specimens. Second, fluorescence images of resected specimens were obtained using the selected probe; these images were used to evaluate the diagnostic accuracy of the spread of cholangiocarcinoma. Finally, the target enzyme was comprehensively explored, and its expression in cholangiocarcinoma was assessed.

Sample Collection

This study was approved by the Institutional Review Board of the University of Tokyo Hospital (IRB No. 2957-[11]). Tissue samples were collected from bile duct specimens that had been surgically resected between May 2018 and December 2020. Written informed consent for sample collection or fluorescence imaging of resected specimen was obtained from all patients.

Enzyme-Activatable Probe Library

Our probe library contains 800 types of enzyme-activatable probes: 384 types of HMRG-based fluorescence probes for peptidases (P1-HMRG or P2-P1-HMRG) [11], 400 types of 2MeSiR-based fluorescence probes for peptidases (2MeSiR probes: P2-P1-2MeSiR) [12, 14], and 16 types of hydroxymethyl rhodol with trifluoroethyl (HMRef)-based fluorescence probes for glycosidases (HMRef probes: monosaccharide-HMRef) [13]. The strategies and structures of these probes are summarized in Figure 1a and online supplementary Figure 1 (for all online suppl. material, see www.karger.com/doi/10.1159/000530645), respectively.

Primary Probe Selection (Assay Using Lysates of Resected Specimens)

An overview of the process from sample collection to primary and secondary probe selection is shown in Figure 1b. The method of primary probe selection is described in detail elsewhere [13, 20, 22]. Briefly, tissue was homogenized with 1.0 mL of T-Per Tissue Protein Extraction Reagent (Pierce) using Lysing Matrix D. After centrifugation at 1,000 rpm for 5 min at 4°C, the supernatant (i.e., lysate) was collected. Then, 5 μL of lysate was added to each well of a 384-well black plate containing 15 μL of each candidate probe from the library. The final probe and lysate protein concentrations for the assay were adjusted to 1.0 μM and 0.050 mg/dL, respectively. After the addition of lysate, the fluorescence intensity (FI) was measured at 2-min intervals for 60 min while the plate was incubated at 37°C, using an Envision Multilabel Plate Reader (PerkinElmer, MA, USA). For lysates in which the protein concentration was low because of insufficient collected tissue, the incubation time was increased in a manner inversely proportional to the protein concentration. The respective excitation and emission wavelengths were 485 nm and 535 nm for HMRG or HMRef probes, and 531 nm and 620 nm for 2MeSiR probes. Because FI did not linearly increase for all probes, the increase in FI was defined as follows:

$$\text{(FI increase) (a.u.)} = \text{(Maximum FI)} - \text{(Minimum FI)}$$

FI was defined as "0" if FI at 60 min was lower than FI at 0 min. During probe selection, we picked candidates that met the following two criteria: the mean FI increase of cancer lysates was (1) sufficiently high by itself and (2) sufficiently higher than the mean FI increases of non-cancer lysates and bile samples. Specific criteria for each fluorophore were as follows. For HMRG probes, (1) the ratio of the mean FI increase of cancer lysates to the FI of HMRG alone was >10%; (2) the ratios of the mean FI increase of cancer lysates to the mean FI increases of non-cancer lysates and bile

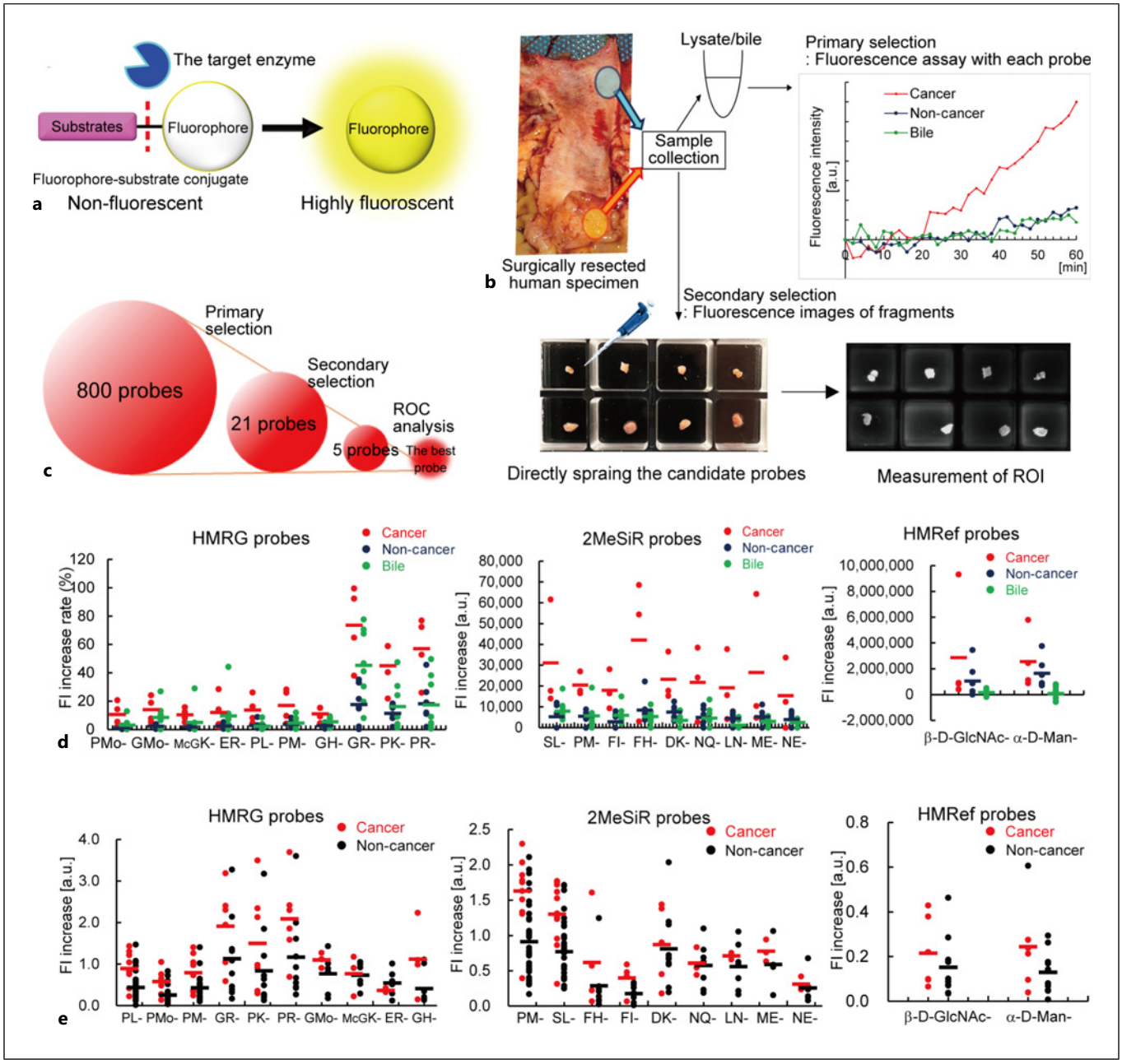

Fig. 1. Details of enzyme-activatable probes, probe selection, and the analysis of FI for candidate probes during primary/secondary selection. **a** Enzyme-activatable fluorescence probe strategy. The probe consists of a fluorophore (HMRG, 2MeSiR, or HMRef) and a substrate (amino acid, dipeptide, or monosaccharide). The initially non-fluorescent probe is hydrolyzed by the target enzyme (aminopeptidase or glucosidase) and emits fluorescence. **b** Overall scheme of probe selection. **c** Outline of sample collection and primary/secondary probe selection. **d** Analysis of the increase in FI for probes that met the criteria for each fluorophore. Values for each cancer lysate, non-cancer lysate, and bile specimen are plotted in red, blue, and green, respectively. Bars indicate mean values. The alphabets, Mo, and MeG represent amino acids (e.g., P: proline), oxidated methionine, and N-methyl glycine (sarcosine), respectively. GlcNAc and Man represent acetylated glucose and mannose, respectively. In the selection of 2MeSiR probes (D, middle), the extremely high values of total FI for a cancer lysate suggested that all probes had already been hydrolyzed at that point; the affected lysate was excluded from probe selection. **e** Secondary probe selection results. FI increases are shown for both cancer (left, red) and non-cancer bile duct (right, black) fragments at 30 min after the application of each candidate probe. Bars indicate median values. The meanings of alphabets, Mo, MeG, GlcNAc, and Man are identical to **d**. C, cancer fragments; N, non-cancer fragments.

samples were ≥3. For 2MeSiR probes, (1) the mean FI increase of cancer lysates was ≥10,000 a.u.; (2) the ratios of the mean FI increase of cancer lysates to the mean FI increases of non-cancer lysates and bile samples were ≥3; (3) the distribution of FI increase in each lysate was small. For HMRef probes, (1) the mean FI increase of cancer lysates was ≥2,000,000 a.u.; (2) the mean FI increases of non-cancer lysates and bile samples were <2,000,000 a.u.; (3) the distribution of FI increase in each lysate was small.

Secondary Probe Selection (Fluorescence Imaging with Small Fragments)

Tissue samples were divided into fragments of a few millimeters and placed in an eight-well plate. Fluorescence images were obtained after candidate fluorescence probes (50 μM, 200 μL) had been directly sprayed using the Maestro in Vivo Imaging System (PerkinElmer); blue filter settings (excitation and emission wavelengths of 435–480 nm and 490 nm long pass) were used for HMRG and HMRef probes, whereas yellow filter settings (excitation and emission wavelengths of 575–621 nm and 635 nm long pass) were used for 2MeSiR probes. Fluorescence images were acquired at 0 (before), 1, 3, 5, 10, 15, 20, and 30 min after the administration of fluorescence probes; the images were extracted at wavelengths of 540 nm (HMRG and HMRef probes) and 640 nm (2MeSiR probes). The FI increase at each time point was calculated by subtracting the mean FI in the region of interest from the mean FI in that region at 1 min. Because some sample sizes were insufficient to obtain fragments for analysis of each candidate probe, probes with little differences in FI increase between a few cancer and non-cancer tissue fragments were sequentially excluded. Probes that showed a significantly greater FI increase in cancer tissues than in non-cancer tissues at 30 min were subjected to receiver operating characteristic analysis and calculation of area under the curve.

Fluorescence Imaging of Whole Surgical Specimens

Immediately after a specimen was resected and the bile duct was opened in the usual manner, fluorescence images were acquired at 0 (before), 1, 3, 5, 10, 15, 20, 25, and 30 min after the selected probe solution (4 mL, 50 μM solution) had been directly sprayed onto the surface of the bile duct, using the Maestro in Vivo Imaging System (PerkinElmer) as described above. Fluorescence images were compared with corresponding pathology findings, and the probe detection accuracy was evaluated by a surgeon (R.T.) and a pathologist (M.T.).

Exploration of Target Enzymes

Diced Electrophoresis Gel Assay

The search for target enzymes that can activate the probe was performed using a diced electrophoresis gel (DEG) assay [23]. Details are provided elsewhere [13, 20, 23]. Briefly, cancer lysates were subjected to two-dimensional electrophoresis under non-denaturing conditions; subsequently, the gel was placed into 384-well black plates for dicing and centrifugation at 3,000 rpm for 5 min. A single fluorescence probe (1.0 μM, 80 μL) was added to each well and the plate was incubated at 37°C for 12 h under sealed conditions. The assay was performed using the Envision Multilabel Plate Reader (PerkinElmer), as described above for primary probe selection. The FI increase for each diced gel was calculated and summarized using a heat map. Diced gels with the highest activity were collected for liquid chromatography coupled with tandem mass spectrometry (LC/MS-MS) analysis.

LC/MS-MS Analysis

Protein digestion and LC/MS-MS-based protein identification (peptide mass fingerprinting analysis) were performed by Integrale Co., Ltd. The resulting LC/MS-MS data were analyzed using the MASCOT Server 2.3 (Matrix Science Ltd.) to identify putative proteins. These proteins were used as queries in an enzyme database (BRENDA; https://www.brenda-enzymes.org/) to identify target enzymes that cleaved the probes.

Enzyme Inhibitor Assay

As in the DEG assay, the same lysate (adjusted to 0.025 mg protein/mL) was incubated with the probe and candidate enzyme inhibitors for 120 min. Based on the results of the DEG assay, LC/MS-MS analysis, and scanning of the enzyme database, E-64 (331-40963, FUJIFILM), amastatin (ab142479, Abcam), SNJ-1945 (Senju Pharmaceutical Co.), calpain inhibitor II (A6060, Sigma-Aldrich), and puromycin (160-23151, FUJIFILM) were separately added to the assay buffer at various final concentrations (0, 0.001, 0.01, 0.1, 1.0, 10, and 100 μM). Other assay protocols were performed using the Envision Multilabel Plate Reader (PerkinElmer), as described above for primary probe selection.

In vitro Fluorescence Analysis with Purified Enzymes

The reactivities of candidate enzymes to the probe were evaluated in vitro. Based on the results of the enzyme inhibitor assay, recombinant human NPEPPS protein (2.5 μg; 6410-ZN, R&D Systems), recombinant human LAP3 protein (10 μg; ab202613, Abcam), recombinant human CNDP2 protein (10 μg; ab139781, Abcam), and recombinant human ERAP1 protein (2.5 μg; 2334-ZN, R&D Systems) were separately added as candidate enzymes. The time course of FI after addition of the enzyme into the probe solution (1.0 μM, 3.0 mL) was measured for 1,000 s using the F-7000 Hitachi Fluorescence Spectrophotometer (Hitachi, Tokyo, Japan). The excitation and emission wavelengths were 495 nm and 525 nm for HMRG/HMRef probes; they were 595 nm and 615 nm for 2MeSiR probes.

Target Enzyme Expression in Cancer Cells

Immunohistochemical Staining

Immunohistochemical (IHC) staining was used to evaluate the gene expression of the target enzyme in resected specimens used for fluorescence imaging. Antigen retrieval was performed at 121°C for 5 min. Based on the results of in vitro fluorescence analysis with purified enzymes, we used a primary antibody specific for NPEPPS (1:275; HPA045649, rabbit, Sigma-Aldrich). The results were evaluated by a pathologist (M.T.).

Western Blotting

The level of enzyme expression was also analyzed by Western blotting. Cryopreserved cancer and non-cancer lysates were diluted to a protein concentration of 0.40 mg/dL, then mixed with sodium dodecyl sulfate buffer and incubated at 95°C for 3 min. Electrophoresis (sodium dodecyl sulfate-polyacrylamide gel electrophoresis, 200 V, 30 min) was performed using 7.0 μL of each lysate; samples were then electrotransferred onto Immobilon-P polyvinylidene difluoride membranes (Millipore) (15 V, 30 min)

and blocked for 1 h (25°C, Tris-buffered saline with Tween-20 containing 5% skim milk). Subsequently, membranes were incubated at 4°C overnight with primary antibody, then at 25°C for 60 min with secondary antibody (see end of paragraph for antibody information). After membranes had been reacted with an enhanced chemiluminescence reagent (ECL, GE Healthcare), protein bands were visualized using an Image Quant LAS 4000 (GE Healthcare); images were analyzed using ImageJ software (National Institutes of Health, Rockville, MD, USA; https://rsbweb.nih.gov/ij/). The primary antibody was identical to the antibody used for IHC: NPEPPS (1:250); an anti-β-actin antibody (1:2,000; A5441, mouse, Sigma-Aldrich) was used as a loading control. Secondary antibodies were anti-rabbit IgG (1:2,000; #7074, Cell Signaling) for NPEPPS and anti-mouse IgG (1;2,000; #7076, Cell Signaling) for β-actin. Can Get Signal Solutions 1 and 2 (Toyobo) were used as buffers for the primary and secondary antibodies to NPEPPS.

Cancer Cell Imaging with/without Knockdown of Target Enzymes

Fluorescence imaging of the human cell line TFK-1 (derived from eCCA) using the selected fluorescence probe was performed with and without the transfection of siRNA designed to knock down the expression of the target enzyme. TFK-1 cells seeded in eight-well plates (Ibidi) were transfected with 10 nmol/L of siRNA targeting NPEPPS (EHU110251, esiRNA human NPEPPS, Sigma-Aldrich) or negative control siRNA (SIC-001, siRNA Universal Negative Control #1, Sigma-Aldrich), diluted in Lipofectamine RNAiMAX transfection reagent (#13778030, Invitrogen). The probe (1.0 μM) was added to the culture medium 48 h after transfection. Cells were incubated at 37°C, and fluorescence imaging was performed 15 min after probe addition. Fluorescence imaging was separately conducted three times for each siRNA. Ten cells were arbitrarily selected, and the regions of interest of images at each time point were measured using ImageJ software (National Institutes of Health).

Statistical Analysis

The FI increase in cancer fragments was compared with the FI increase in non-cancer fragments by the Wilcoxon rank-sum test during secondary probe selection. $p < 0.05$ was considered statistically significant. Statistical analysis was performed using JMP Pro software (version 16.0.0; SAS Institute Inc., Cary, NC, USA).

Results

Probe Selection

The overall results of probe selection are summarized in Figure 1c. For primary probe selection, we used four cancer lysates, seven non-cancer lysates, and eight bile samples from 10 patients (online suppl. Table 1). In total, 21 candidate probes (10 HMRG probes, nine 2MeSiR probes, and two HMRef probes) met the criteria for each fluorophore and were selected as candidates (shown in Fig. 1d; online suppl. Fig. 2). For secondary probe selection, 13 cancer fragments and 41 non-cancer bile duct fragments were collected from 45 patients (13 patients with eCCA and 32 patients with non-cholangiocarcinoma) (shown in online suppl. Table 2; Fig. 1e). Consequently, five probes (PM-2MeSiR, SL-2MeSiR, PMo-HMRG, PL-HMRG, and PM-HMRG) showed a significant difference between the FI increase in cancer fragments and the FI increase in non-cancer fragments at 30 min after probe application (shown in Fig. 1e, 2a). Of those, PM-2MeSiR exhibited the highest area under the curve (shown in Fig. 2a) and was selected as the cancer-specific probe. The structure of this probe and individual data concerning secondary probe selection are summarized in Figure 2b–e.

Fluorescence Imaging of Whole Surgical Specimens Using the Candidate Probe

Seven resected specimens were subjected to fluorescence imaging with PM-2MeSiR. The patient characteristics and the results of fluorescence imaging are summarized in Table 1. The main lesion of the tumor was visible as an area of strong fluorescence in all cases. In 4 cases, the spread of cholangiocarcinoma almost coincided with the area of fluorescence; in the other 3 cases, some false-positive and false-negative areas were observed. Figures 3 and 4 show fluorescence images of the resected specimens of patients 1 and 2, respectively. In the specimen of patient 1, who underwent pancreaticoduodenectomy for distal cholangiocarcinoma, the area of strong fluorescence almost coincided with the spread of cholangiocarcinoma that was difficult to detect macroscopically; however, there were small areas of fluorescence in the common hepatic duct where cholangiocarcinoma had not invaded. In the specimen of patient 2, who underwent the resection of remnant anterior section for hilar cholangiocarcinoma, the main lesion was strongly fluorescent and the common tract of the posterior branch and dorsal branch of segment 8 (B6+7+8dor) was a true-negative area. However, fluorescence was weak around the stump of the common bile duct where cholangiocarcinoma had invaded. The fluorescence imaging results of the other five specimens are shown in online supplementary Figure 3.

Exploration of Enzymes Able to Cleave PM-2MeSiR

Two hot spots were observed in all DEG assays (shown in Fig. 5a). LC-MS/MS analysis and subsequent database exploration detected several types of candidate enzymes in each hot spot (shown in Fig. 5a; online suppl. Tables 3, 4). Fluorescence assays using enzyme inhibitors showed that low concentrations of amastatin and puromycin could suppress the FI increase (shown in Fig. 5b).

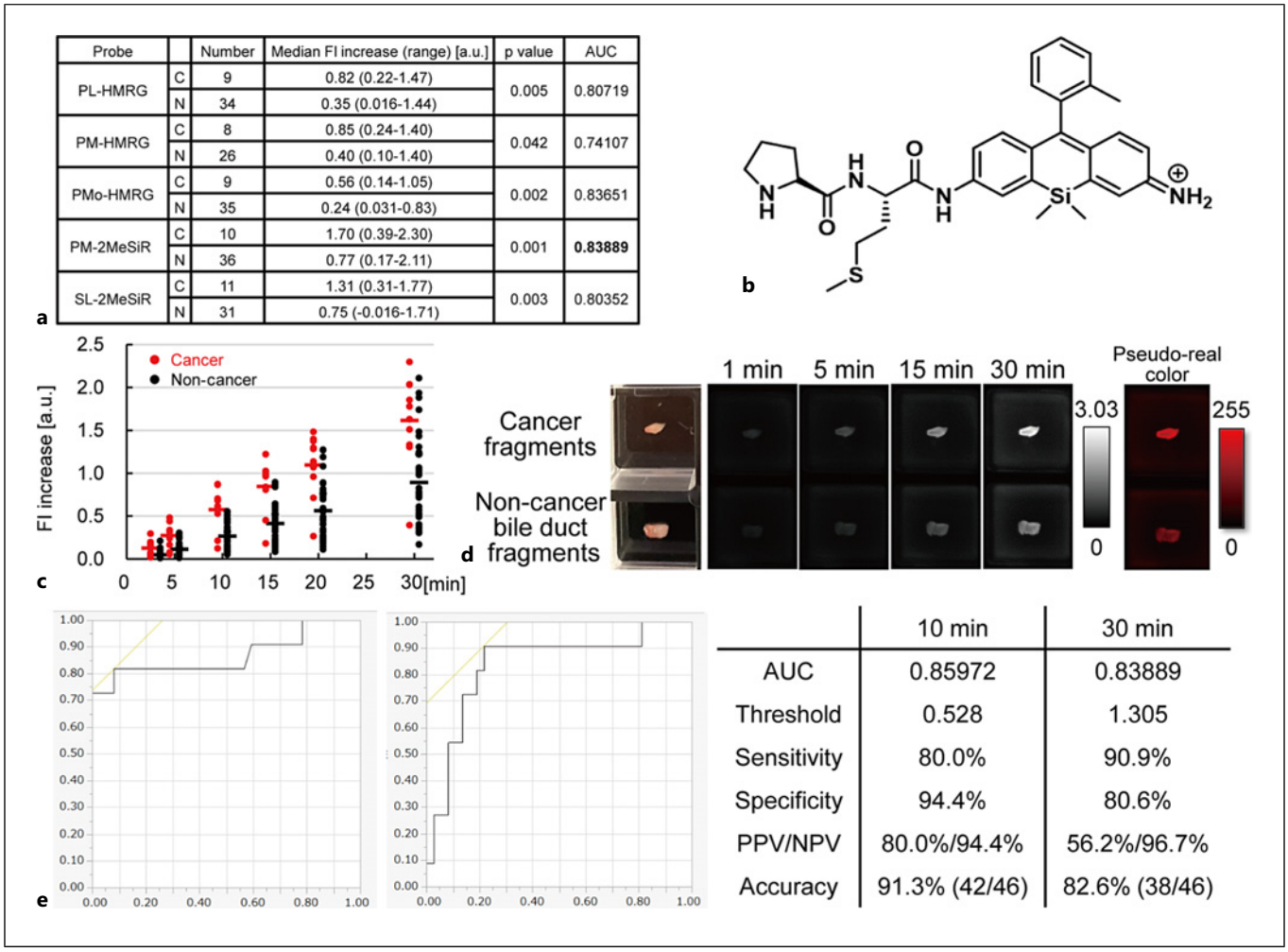

Probe		Number	Median FI increase (range) [a.u.]	p value	AUC
PL-HMRG	C	9	0.82 (0.22-1.47)	0.005	0.80719
	N	34	0.35 (0.016-1.44)		
PM-HMRG	C	8	0.85 (0.24-1.40)	0.042	0.74107
	N	26	0.40 (0.10-1.40)		
PMo-HMRG	C	9	0.56 (0.14-1.05)	0.002	0.83651
	N	35	0.24 (0.031-0.83)		
PM-2MeSiR	C	10	1.70 (0.39-2.30)	0.001	**0.83889**
	N	36	0.77 (0.17-2.11)		
SL-2MeSiR	C	11	1.31 (0.31-1.77)	0.003	0.80352
	N	31	0.75 (-0.016-1.71)		

Fig. 2. Probe selection and individual results for selected probes obtained during secondary probe selection. **a** Results of receiver operating characteristic analysis of the final five selected probes. The area under the curve (AUC, five significant digits) was highest for PM-2MeSiR. **b** Structure of PM-2MeSiR. **c** Time course of PM-2MeSiR FI for cancer (left, red) and non-cancer bile duct (right, black) fragments. Bars indicate median values. **d** Fluorescence image (640 nm) and pseudo-real color images (600–800 nm) of cancer and non-cancer bile duct fragments. **e** ROC curve at 10 min (left) and 30 min (middle) after the application of PM-2MeSiR. AUC and other data are shown in the table (right).

Thus, puromycin-sensitive aminopeptidase (PSA; NPEPPS), cytosol aminopeptidase (LAP3), cytosolic non-specific dipeptidase (CNDP2), and endoplasmic reticulum aminopeptidase (ERAP1) were identified as candidate enzymes (genes). In vitro protein assays revealed that only human recombinant PSA could activate PM-2MeSiR (shown in Fig. 5c).

PSA Expression in Cancer Cells

IHC staining revealed that NPEPPS expression was slightly elevated in cancer cells, compared with that in non-cancerous bile duct epithelium in tissues from 4 patients such as patient 1 (shown in Fig. 6a). In contrast, there was no clear difference in NPEPPS expression between cancer and non-cancer cells in tissues from other patients such as patient 2 (shown in Fig. 6b). Western blotting revealed that NPEPPS protein was overexpressed in both of two cancer lysates, compared with that in three non-cancer lysates including one lysate of bile ducts from a patient with primary sclerosing cholangitis (shown in Fig. 6c). In live-cell imaging of TFK-1 (derived from eCCA), cancer cells with knockdown of PSA were less fluorescent than control cells or cells with negative siRNA (shown in Fig. 6d).

Table 1. Patient characteristics and summary of fluorescence imaging findings

No.	Age, years	Sex	Main site of the lesion	Procedure	Fluorescence of main lesion	Histological type	Fluorescence at the stump of the bile duct	The FP/FN area
1	79	Male	Distal	Pancreaticoduodenectomy	Strong	pap, tub1 > tub2	TN	Almost none
2	75	Male	Hilar	The resection of remnant anterior section	Strong	tub2 > por	Posterior duct: TN CBD: FN	CBD (FN)
3	55	Male	Distal	Pancreaticoduodenectomy	Strong	por > tub1 > tub2	TN	None
4	78	Male	Distal	Pancreaticoduodenectomy	Strong	tub1	TN	None
5	65	Male	Hilar	Extended right hemi-hepatectomy	Strong	tub1 > tub2	LHD: TP CBD: FP	CBD (FP)
6	85	Female	Hilar	Extended right hemi-hepatectomy	Strong	tub2 > tub1 > por	LHD: TN CBD: TN	None
7	77	Male	Hilar	Extended right hemi-hepatectomy	Strong	tub1 > tub2 > por	LHD: TN CBD: FN	CBD (FN)

TN, true negative; TP, true positive; FN, false negative; FP, false positive; CBD/CHD, common bile/hepatic duct; LHD, left hepatic duct; tub1/tub2/por, well/moderately/poorly differentiated adenocarcinoma; pap, papillary adenocarcinoma.

Discussion

In this study of 800 candidate enzyme-activatable fluorescence probes, PM-2MeSiR was identified as the most promising fluorescent probe that enabled real-time identification of eCCA. Subsequent analyses suggested that PSA is the target enzyme of PM-2MeSiR.

The cancer identification method described in this study, based on topical administration of enzyme-activatable fluorescence probes, has potential advantages such as ease of preparation, high tumor-to-background ratio, and intraoperative visualization during surgery. Indeed, related techniques that involve enzyme-activatable probes have been used in clinical trials for surgical treatment of breast cancer [15] and esophageal cancer [16]. In terms of fluorescence imaging for eCCA, a few reports are available concerning the use of a fluorescence probe that targets the GLUT receptor [24] and 5-aminolevulinic acid [25]. However, these techniques have not yet been used in clinical practice because they require optimization of the wash-out period (interval between systemic probe administration and observation) to obtain intraoperative images with a sufficiently high tumor-to-background ratio. In contrast, our technique involving the topical administration of enzyme-activatable probes may be useful for endoscopic examinations, as well as intraoperative diagnosis of eCCA, because we excluded fluorescent probes that can be activated by bile.

Fluorescence imaging with PM-2MeSiR is expected to enable accurate identification of the spread of superficial cancer in the biliary system, which would facilitate decisions concerning surgical indications and operative procedures. For example, pre- or intraoperative assessment of longitudinal cancer spread by fluorescence cholangioscopy after intraductal injection of the fluorophore may be useful in such decisions. Although the topical administration of our fluorescence probes may be hindered by low tissue penetration, submucosal invasion can be detected by intraoperative fluorescence imaging if the probe is sprayed onto bile duct stumps or the transected surfaces of bile duct walls; such detection may enhance the accuracy and feasibility of existing methods for confirmation of surgical curability, which are mainly based on rapid intraoperative pathological diagnosis. In the future, if enzyme-activatable probes can be sprayed into the abdominal cavity, fluorescence imaging may be able to detect intraductal spread, along with perineural invasion and lymph node metastases outside of bile ducts, as demonstrated in patients with pancreatic cancer [22] and breast cancer [16].

In the present study, DEG assay and inhibitor studies suggested that PSA was the most likely target enzyme for PM-2MeSiR activation. Western blotting and cancer cell imaging with/without knockdown of PSA also suggested the overexpression of PSA in cancer tissues, compared with non-cancer bile ducts. Although IHC staining showed minimal differences in PSA expression between cancer cells and non-cancer cells, this discrepancy may have occurred because enzyme activity does not always correspond to the protein expression level determined by

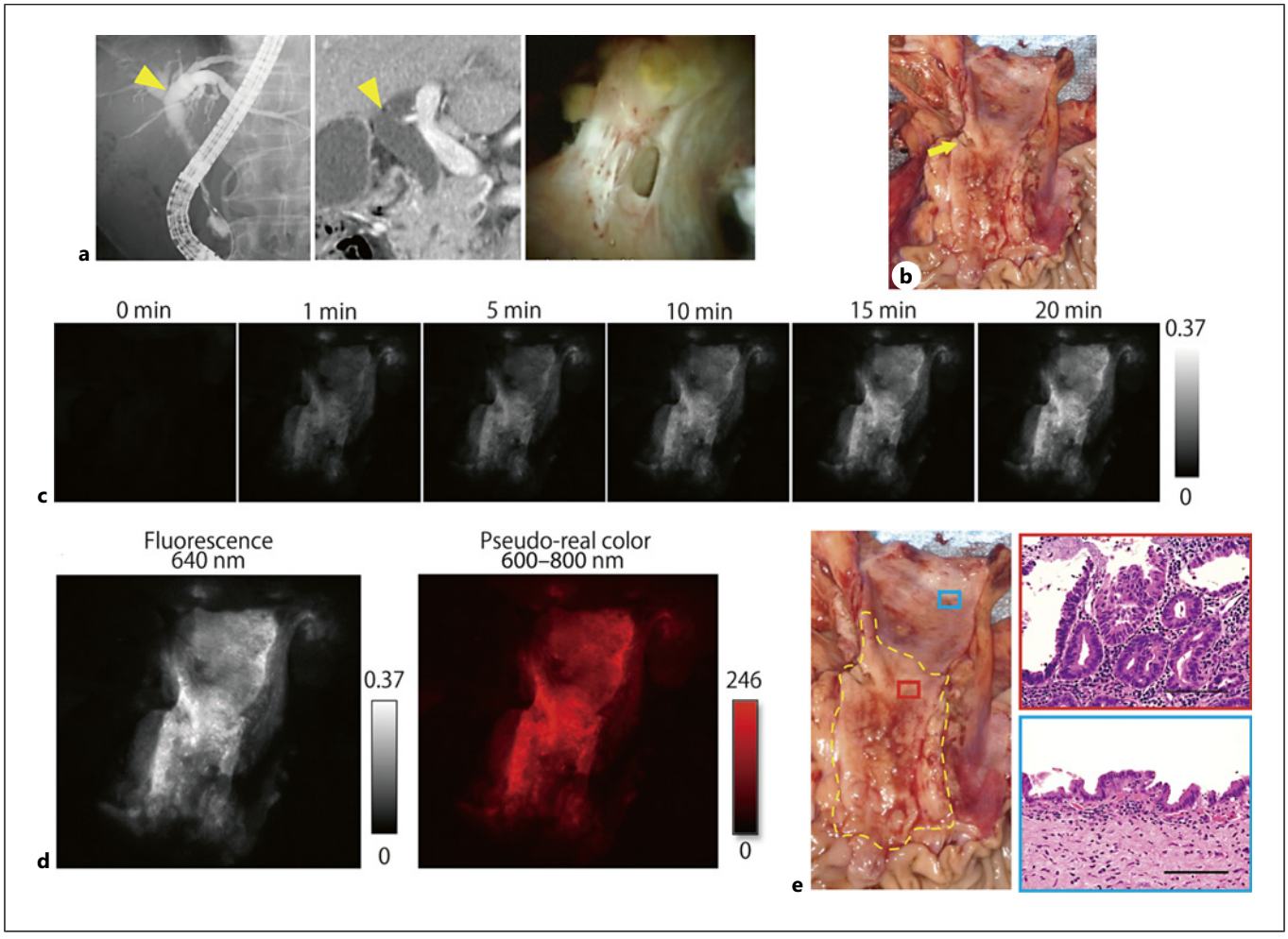

Fig. 3. Fluorescence imaging of resected specimen from patient 1, who underwent pancreaticoduodenectomy for distal cholangiocarcinoma. **a** Preoperative images of endoscopic retrograde cholangiography (ERC, left), contrast-enhanced computed tomography (CECT, middle), and cholangioscopy (right). The bile duct is dilated because of stenosis with wall thickening in the distal bile duct. However, mapping biopsy of the confluence of the right and left hepatic ducts (arrowhead), which showed abnormal epithelium on cholangioscopy (right), indicated positive findings, which hindered the diagnosis of longitudinal spread of cholangiocarcinoma. **b** Macroscopic findings of the resected specimen. The hepatic duct was transected at the level of the confluence of the right and left hepatic ducts. A papillary neoplasm is visible in the distal bile duct, but its spread over the cystic duct (arrow) is unclear. **c** Time course of fluorescence images (640 nm) (from 1 min to 20 min). **d** Fluorescence image (640 nm) and pseudo-real color image (600–800 nm) at 30 min. The area of fluorescence includes the papillary lesion, as well as the confluence of cystic ducts. A small area of fluorescence was also visible around the right side of the incision stump of the common hepatic duct. **e** Pathology findings of the resected specimen. The yellow dotted line shows the spread of pathologically detected cholangiocarcinoma, which almost coincided with the strongly fluorescent area. However, the small area of fluorescence at the common hepatic duct was a false-positive area. Area of strong fluorescence (red) indicates the presence of cancer cells, while the area of weak fluorescence (blue) indicates normal bile duct epithelium. Scale bar, 100 μm.

IHC, presumably because of post-transcriptional modification. PSA is an aminopeptidase with broad substrate specificity; it is reportedly involved in proteolytic events that are essential for cell growth and viability, including the antigen processing pathway for MHC class I molecules [26]. Furthermore, PSA overexpression has been reported in prostate cancer and renal cancer [27, 28]. In the context of eCCA, however, there have been few reports of overexpression concerning PSA or other enzymes. Additionally, it is unclear whether enzyme activities in vivo are directly linked to the corresponding expression levels. Enzyme-activatable fluorescence

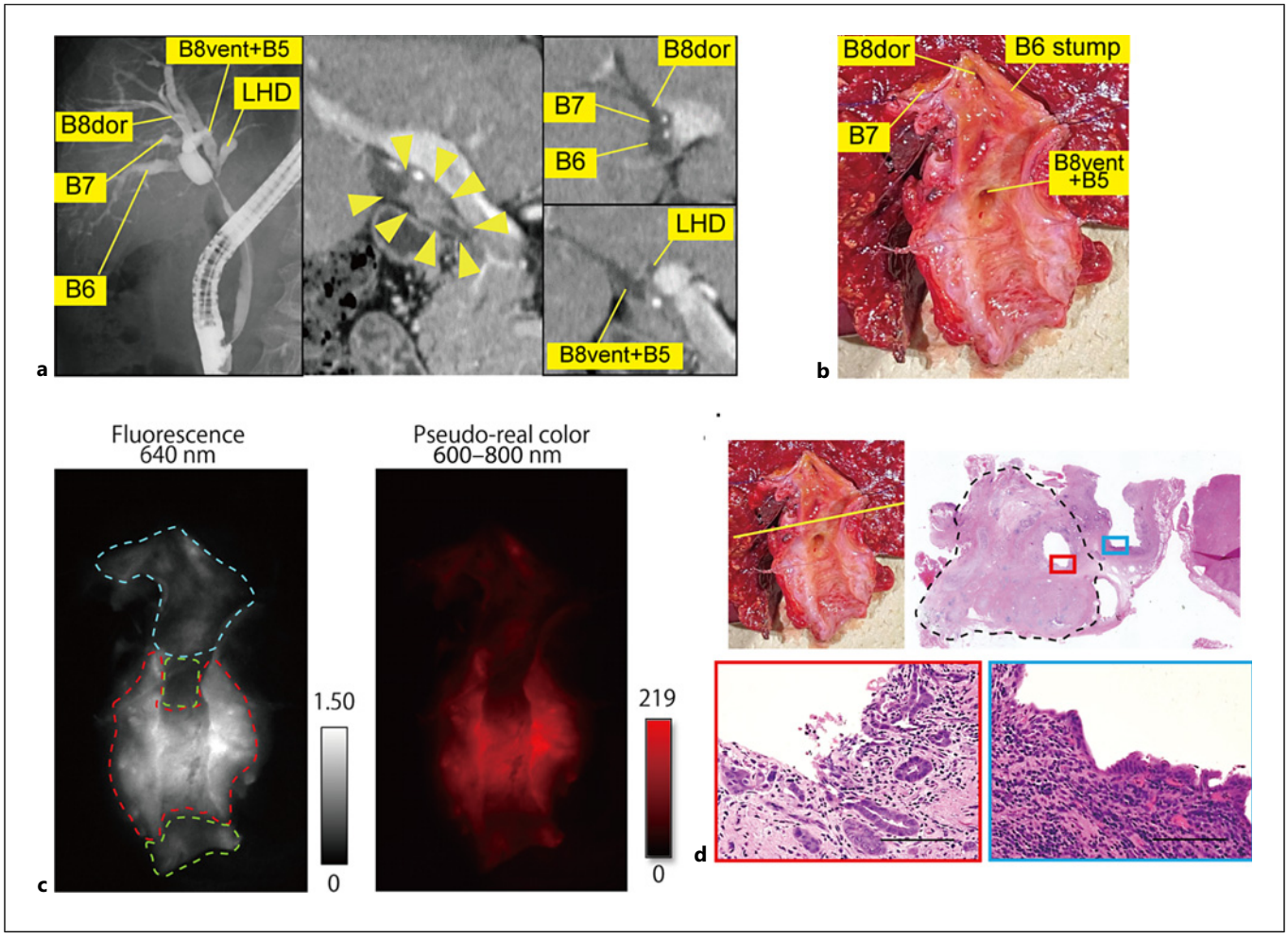

Fig. 4. Fluorescence imaging of resected specimen from patient 2, who underwent remnant anterior sectionectomy for hilar cholangiocarcinoma after left hemi-hepatectomy for intrahepatic stones. **a** Preoperative ERC (left) and CECT (middle and right). ERC findings showed that the dorsal branch of B8 (B8dor) was independently joined to the posterior branch (B6+7). The common trunk of B8dor and the posterior branch was dilated without irregularity and remained completely separate from another common trunk of the ventral branch of B8 (B8vent), B5, and remnant left hepatic duct (LHD). CT findings showed enhanced wall thickening at the common hepatic duct (arrowheads), which did not appear to have spread to the intrapancreatic bile duct. The confluence of B8dor and the posterior branch appeared to be intact (right, above), whereas cholangiocarcinoma appeared to have spread to the confluence of the left hepatic duct and B8vent+B5 (right, below). **b** Macroscopic findings of the resected specimen. The bile duct was transected at the level of the pancreatic head and at the confluence of B8dor and the posterior branch. The site of wall thickening was consistent with preoperative images. **c** Fluorescence images (640 nm) and pseudo-real color image (600–800 nm) at 30 min. The main lesion showed an area of strong fluorescence, whereas other areas exhibited weak fluorescence. Pathology findings revealed some true-positive (main lesion, red dotted line) and true-negative areas (common trunk of B8dor and posterior branch, blue dotted line), as well as false-negative areas (confluence of posterior and anterior branches and the common bile duct, green). **d** HE staining of the resected specimen. Specimen at the yellow line (above), where fluorescence was weak, included both deep cancerous tissue (red) and shallow non-cancerous tissue (blue). Black dotted lines indicate the spread of cancer. Scale bar, 100 μm.

probes have facilitated assessments of enzyme activities [10–22]. Therefore, we identified the most promising probe in our library, then comprehensively evaluated the target enzyme using a published approach [11, 14, 20]. Our strategy of identifying cancer-specific enzymes via fluorescence imaging with activatable probes may lead to real-time diagnosis, as well as the exploration of new therapeutic targets [26, 29] and prediction of sensitivity to adjuvant therapy and postoperative outcomes, similar to previous work

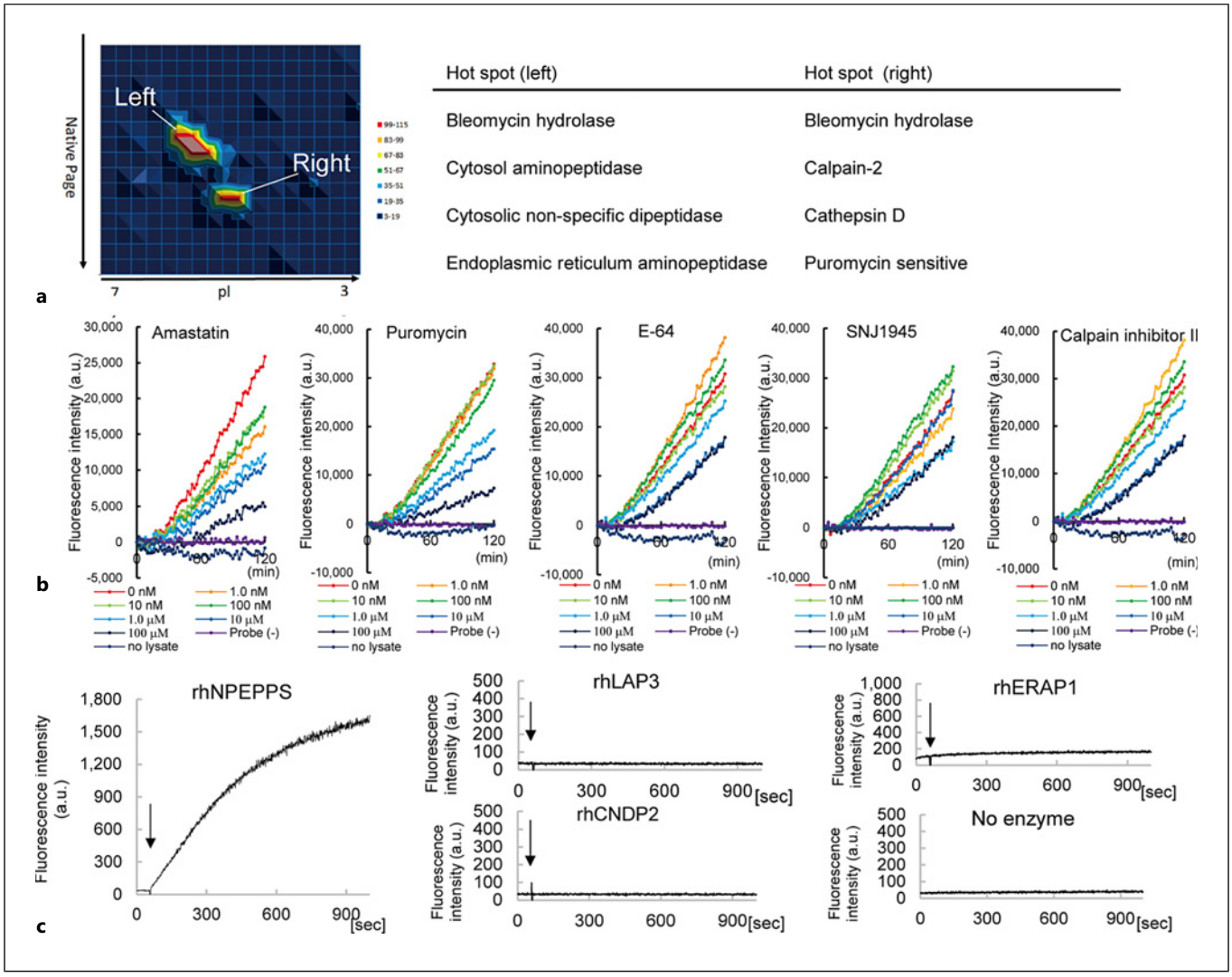

Fig. 5. Exploration of the target enzyme. **a** DEG assay hot spots (left) and candidate enzymes acquired from the enzyme database for each spot (right). **b** Fluorescence assay using a cancer lysate and PM-2MeSiR with various concentrations of inhibitors. Low concentrations of amastatin and puromycin inhibited PM-2MeSiR activation. **c** Time course of FI after addition of purified recombinant human (rh-) enzyme in vitro. Only the rhNPEPPS protein could activate PM-2MeSiR.

involving lung, liver, esophageal, and renal cancers [18, 21, 30–32].

This study had a major limitation in terms of the small sample sizes used for probe selection and fluorescence imaging, which may have led us to overlook enzyme-activatable probes that are superior to PM-2MeSiR for real-time visualization of eCCA. Because it is usually challenging to identify a large number of surgical cases with sufficient tissue sample volumes among patients with relatively rare diseases, we plan to continue evaluating the diagnostic abilities of fluorescence imaging with PM-2MeSiR and other candidate probes in multicenter trials and/or non-clinical studies using animal models [24], organoids [33], and patient-derived xenografts [34] of eCCA. There is also a need to establish a method for quantitative evaluation of cancer spread via fluorescence imaging. Although it is possible to measure the FI of each cancerous and non-cancerous region, the accuracy of this approach has not been confirmed. Furthermore, we might also have missed other cancer-specific enzymes that could activate PM-2MeSiR. In particular, candidate enzymes in the other hot spot in the DEG assay might

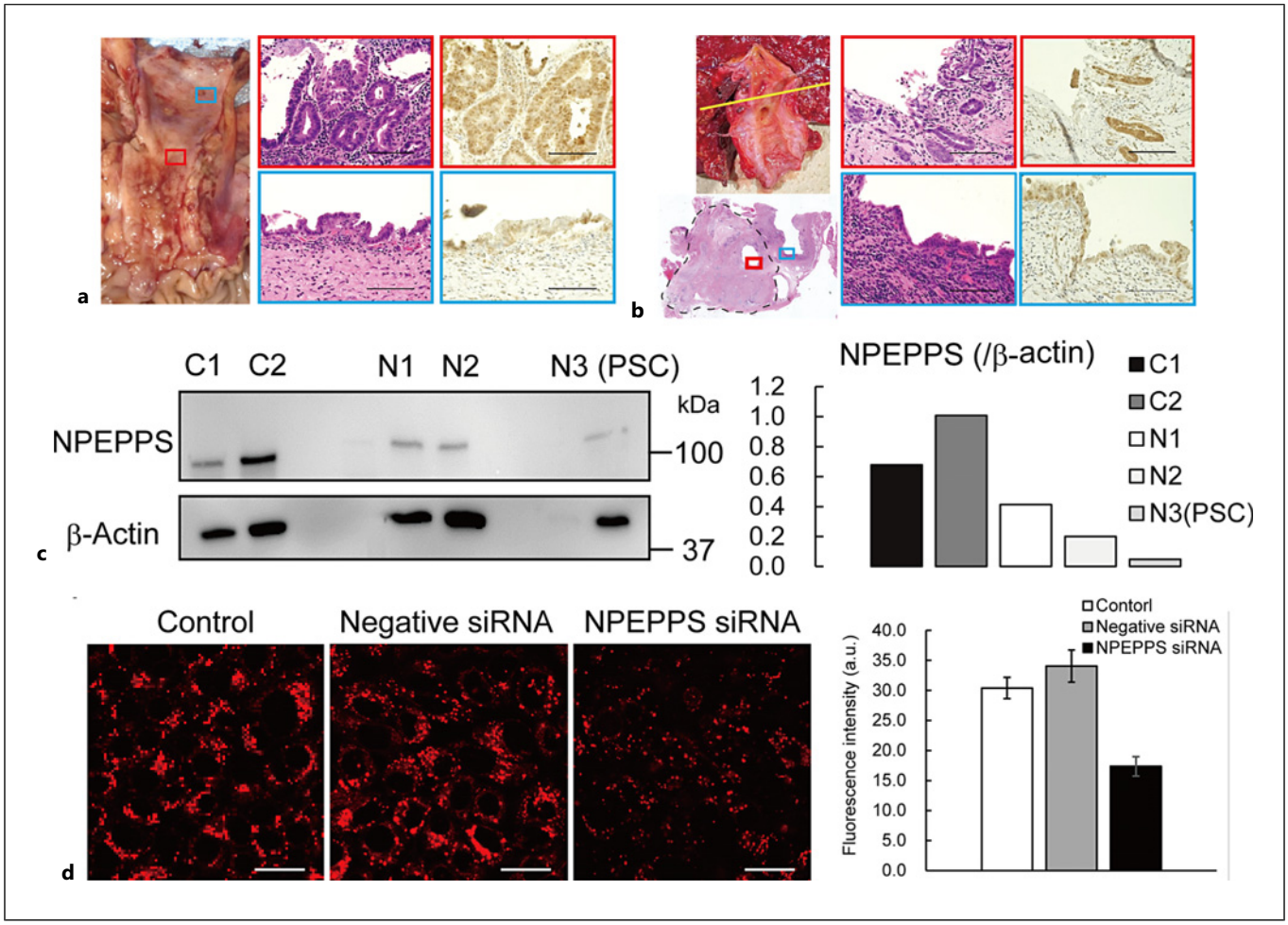

Fig. 6. Expression levels of target enzymes in cancerous and non-cancerous tissues and live-cell imaging of TFK-1 cells with knockdown siRNA. **a**, **b** HE and immunohistochemical (IHC) staining of resected specimens from patients 1 and 2. In patient 1, NPEPPS expression was only slightly elevated in cancer cells, compared with non-cancer bile duct; in patient 2, there was no clear difference in NPEPPS expression between cancer and non-cancer cells. Scale bar, 100 μm. **c** Western blotting results. Protein bands (left) and quantitative assessment (right) revealed that NPEPPS expression was upregulated in cholangiocarcinoma. **d** Fluorescence images of TFK-1 cells with and without knockdown siRNA of target enzyme at 15 min (left). NPEPPS siRNA reduced the FI of TFK-1 cells, compared with control cells and cells treated with negative siRNA (right).

have been overlooked in during data exploration or because of recombinant protein inactivation in the in vitro fluorescence assay. Although PM-2MeSiR was identified as the most promising probe in the present study, more effective fluorophores targeting PSA or other cancer-specific enzymes may be identified in future studies with larger numbers of tissue specimens; we presume that such fluorophores would further enhance the accuracy of cancer imaging. Future studies using enzyme-specific fluorescence probes may elucidate target enzymes for fluorescence imaging of eCCA and its exact location in cancerous tissues.

In conclusion, fluorescence imaging after topical administration of PM-2MeSiR may enable real-time assessment of the spread of eCCA during endoscopic diagnosis and surgical treatments, presumably through probe cleavage by PSA that is overexpressed in cancerous tissues. Although larger studies are needed to explore diagnostic ability and target enzymes, our strategy of applying a library of enzyme-activatable probes onto surgically resected tissue specimens may be useful in the development of intraoperative fluorescence imaging techniques and identification of new targets for anticancer therapy.

Acknowledgments

We thank Ryan Chastain-Gross, Ph.D., from Edanz (https://jp.edanz.com/ac) for editing a draft of the manuscript.

Statement of Ethics

"This study protocol was reviewed and approved by the Institutional Review Board of the University of Tokyo Hospital, approval number 2957-(11)." Written informed consent for sample collection or fluorescence imaging of resected specimen was obtained from all patients.

Conflict of Interest Statement

We certify that all pit affiliations or financial involvement with any organization or financial conflict with the subject matter discussed in the manuscript are completely disclosed in the Acknowledgments section of the manuscript.

Funding Sources

T.I. received research funding from the University of Tokyo and NIPRO Corporation. Y.U. received a research grant from the Ministry of Education, Culture, Sports, Science and Technology of Japan (Grant No. 19H05632 to Y.U.)

Author Contributions

All authors contributed to the intellectual content of the manuscript and approved its submission for publication. R.T. and T.I. drafted the initial manuscript. R.T. performed sample collection, data acquisition, statistics, and other analyses. Y.K., K.F., A.O., and M.K. prepared a library of activatable fluorescence probes. R.T. and M.T. evaluated tumor pathology. R.T. and Y.I. performed immunohistochemistry and M.T. evaluated the results. M.K., T.U., Y.U., and K.H. critically evaluated and revised the manuscript.

Data Availability Statement

All data generated or analyzed during this study are included in this article and its supplementary material files. Further inquiries can be directed to the corresponding author.

References

1 Nagino M, Ebata T, Yokoyama Y, Igami T, Sugawara G, Takahashi Y, et al. Evolution of surgical treatment for perihilar cholangiocarcinoma: a single-center 34-year review of 574 consecutive resections. Ann Surg. 2013 Jul;258(1):129–40.
2 Aoki T, Sakamoto Y, Kohno Y, Akamatsu N, Kaneko J, Sugawara Y, et al. Hepatopancreaticoduodenectomy for biliary cancer: strategies for near-zero operative mortality and acceptable long-term outcome. Ann Surg. 2018 Feb;267(2):332–7.
3 Song SC, Choi DW, Kow AW, Choi SH, Heo JS, Kim WS, et al. Surgical outcomes of 230 resected hilar cholangiocarcinoma in a single centre. ANZ J Surg. 2013 Apr;83(4):268–74.
4 Akamatsu N, Sugawara Y, Hashimoto D. Surgical strategy for bile duct cancer: advances and current limitations. World J Clin Oncol. 2011 Feb 10;2(2):94–107.
5 Okuda Y, Taura K, Seo S, Yasuchika K, Nitta T, Ogawa K, et al. Usefulness of operative planning based on 3-dimensional CT cholangiography for biliary malignancies. Surgery. 2015 Nov;158(5):1261–71.
6 Ito K, Sakamoto Y, Isayama H, Nakai Y, Watadani T, Tanaka M, et al. The impact of MDCT and endoscopic transpapillary mapping biopsy to predict longitudinal spread of extrahepatic cholangiocarcinoma. J Gastrointest Surg. 2018 Sep;22(9):1528–37.
7 Navaneethan U, Hasan MK, Lourdusamy V, Njei B, Varadarajulu S, Hawes RH. Single-operator cholangioscopy and targeted biopsies in the diagnosis of indeterminate biliary strictures: a systematic review. Gastrointest Endosc. 2015 Oct;82(4):608–14.e2.
8 Yodice M, Choma J, Tadros M. The expansion of cholangioscopy: established and investigational uses of SpyGlass in biliary and pancreatic disorders. Diagnostics. 2020 Feb 29;10(3):132.
9 Igami T, Nagino M, Oda K, Nishio H, Ebata T, Yokoyama Y, et al. Clinicopathologic study of cholangiocarcinoma with superficial spread. Ann Surg. 2009 Feb;249(2):296–302.
10 Urano Y, Sakabe M, Kosaka N, Ogawa M, Mitsunaga M, Asanuma D, et al. Rapid cancer detection by topically spraying a γ-glutamyltranspeptidase-activated fluorescent probe. Sci Transl Med. 2011 Nov 23;3(110):110ra119.
11 Kuriki Y, Yoshioka T, Kamiya M, Komatsu T, Takamaru H, Fujita K, et al. Development of a fluorescent probe library enabling efficient screening of tumour-imaging probes based on discovery of biomarker enzymatic activities. Chem Sci. 2022 Mar 21;13(16):4474–81.
12 Ogasawara A, Kamiya M, Sakamoto K, Kuriki Y, Fujita K, Komatsu T, et al. Red fluorescence probe targeted to dipeptidylpeptidase-IV for highly sensitive detection of esophageal cancer. Bioconjug Chem. 2019 Apr 17;30(4):1055–60.
13 Fujita K, Kamiya M, Yoshioka T, Ogasawara A, Hino R, Kojima R, et al. Rapid and accurate visualization of breast tumors with a fluorescent probe targeting α-mannosidase 2C1. ACS Cent Sci. 2020 Dec 23;6(12):2217–27.
14 Kawashima S, Yoshida D, Yoshioka T, Ogasawara A, Fujita K, Yanagiya M, et al. Rapid imaging of lung cancer using a red fluorescent probe to detect dipeptidyl peptidase 4 and puromycin-sensitive aminopeptidase activities. Sci Rep. 2022 Jun 1;12(1):9100.
15 Ueo H, Shinden Y, Tobo T, Gamachi A, Udo M, Komatsu H, et al. Rapid intraoperative visualization of breast lesions with γ-glutamyl hydroxymethyl rhodamine green. Sci Rep. 2015 Jul 13;5:12080.
16 Shinden Y, Ueo H, Tobo T, Gamachi A, Utou M, Komatsu H, et al. Rapid diagnosis of lymph node metastasis in breast cancer using a new fluorescent method with γ-glutamyl hydroxymethyl rhodamine green. Sci Rep. 2016 Jun 9;6:27525.
17 Onoyama H, Kamiya M, Kuriki Y, Komatsu T, Abe H, Tsuji Y, et al. Rapid and sensitive detection of early esophageal squamous cell carcinoma with fluorescence probe targeting dipeptidylpeptidase IV. Sci Rep. 2016 Jun 1;6:26399.

18 Kawashima S, Yoshioka T, Hino H, Kitano K, Nagayama K, Sato M, et al. γ-glutamyl hydroxymethyl rhodamine green fluorescence as a prognostic indicator for lung cancer. Gen Thorac Cardiovasc Surg. 2020 Dec;68(12):1418–24.
19 Mizushima T, Ohnishi S, Shimizu Y, Hatanaka Y, Hatanaka KC, Kuriki Y, et al. Rapid detection of superficial head and neck squamous cell carcinoma by topically spraying fluorescent probe targeting dipeptidyl peptidase-IV. Head Neck. 2018 Jul;40(7):1466–75.
20 Kitagawa Y, Tanaka S, Kamiya M, Kuriki Y, Yamamoto K, Shimizu T, et al. A novel topical fluorescent probe for detection of glioblastoma. Clin Cancer Res. 2021 Jul 15;27(14):3936–47.
21 Miyata Y, Ishizawa T, Kamiya M, Yamashita S, Hasegawa K, Ushiku A, et al. Intraoperative imaging of hepatic cancers using γ-glutamyltranspeptidase-specific fluorophore enabling real-time identification and estimation of recurrence. Sci Rep. 2017 Jun 14;7(1):3542.
22 Takahashi R, Ishizawa T, Sato M, Inagaki Y, Takanka M, Kuriki Y, et al. Fluorescence imaging using enzyme-activatable probes for real-time identification of pancreatic cancer. Front Oncol. 2021 Aug 19;11:714527.
23 Komatsu T, Hanaoka K, Adibekian A, Yoshioka K, Terai T, Ueno T, et al. Diced electrophoresis gel assay for screening enzymes with specified activities. J Am Chem Soc. 2013 Apr 24;135(16):6002–5.
24 Yokoyama H, Sasaki A, Yoshizawa T, Kijima H, Hakamada K, Yamada K. Imaging hamster model of bile duct cancer in vivo using fluorescent L-glucose derivatives. Hum Cell. 2016 Jul;29(3):111–21.
25 Fujiwara H, Takahara N, Tateishi K, Tanaka M, Kanai S, Kato H, et al. 5-Aminolevulinic acid-mediated photodynamic activity in patient-derived cholangiocarcinoma organoids. Surg Oncol. 2020 Dec;35:484–90.
26 Hitzerd SM, Verbrugge SE, Ossenkoppele G, Jansen G, Peters GJ. Positioning of aminopeptidase inhibitors in next generation cancer therapy. Amino Acids. 2014 Apr;46(4):793–808.
27 Varona A, Blanco L, López JI, Gil J, Agirregoitia E, Irazusta J, et al. Altered levels of acid, basic, and neutral peptidase activity and expression in human clear cell renal cell carcinoma. Am J Physiol Renal Physiol. 2007 Feb;292(2):F780–8.
28 Lee SH, Kim HG. Cobalt chloride-induced downregulation of puromycin-sensitive aminopeptidase suppresses the migration and invasion of PC-3 cells. J Microbiol Biotechnol. 2009 May;19(5):530–6.
29 Lindberg J, Nilvebrant J, Nygren PÅ, Lehmann F. Progress and future directions with peptide-drug conjugates for targeted cancer therapy. Molecules. 2021 Oct 5;26(19):6042.
30 Zhang JB, Chen Y, Zhang B, Xie X, Zhang L, Ge N, et al. Prognostic significance of serum gamma-glutamyl transferase in patients with intermediate hepatocellular carcinoma treated with transcatheter arterial chemoembolization. Eur J Gastroenterol Hepatol. 2011 Sep;23(9):787–93.
31 Yang F, Zhang S, Yang H, Luo K, Wen J, Hu Y, et al. Prognostic significance of gamma-glutamyltransferase in patients with resectable esophageal squamous cell carcinoma. Dis Esophagus. 2015 Jul;28(5):496–504.
32 Hofbauer SL, Stangl KI, de Martino M, Lucca I, Haitel A, Shariat SF, et al. Pretherapeutic gamma-glutamyltransferase is an independent prognostic factor for patients with renal cell carcinoma. Br J Cancer. 2014 Oct 14;111(8):1526–31.
33 Maier CF, Zhu L, Nanduri LK, Kühn D, Kochall S, Thepkaysone ML, et al. Patient-derived organoids of cholangiocarcinoma. Int J Mol Sci. 2021 Aug 12;22(16):8675.
34 Saito Y, Muramatsu T, Kanai Y, Ojima H, Sukeda A, Hiraoka N, et al. Establishment of patient-derived organoids and drug screening for biliary tract carcinoma. Cell Rep. 2019 Apr 23;27(4):1265–76.e4.